Available online at www.sciencedirect.com
ScienceDirect
Microelectronics Reliability 48 (2008) 569–577
MICROELECTRONICS RELIABILITY
www.elsevier.com/locate/microrel

Effects of length scaling on electromigration in dual-damascene copper interconnects

M.H. Lin [a,b,*], M.T. Lin [b], Tahui Wang [a]

[a] Department of Electronics Engineering, National Chiao-Tung University, Hsin-Chu, Taiwan
[b] United Microelectronics Corporation, No. 3, Li-Hsin Road II, Science-Based Industrial Park, Hsin-Chu 30077, Taiwan

Received 5 March 2007; received in revised form 29 October 2007
Available online 31 December 2007

Abstract

The electromigration short-length effect in dual-damascene Cu interconnects has been investigated through experiments on lines of various lengths (L), being stressed at a variety of current densities (j), and using a technologically realistic three-level structure. This investigation represents a complete study of the short-length effect after a well-developed dual-damascene Cu process. Lifetime measurement and resistance degradation as a function of time were used to describe this phenomenon. It has been found that the sigma of log–normal distribution increased as the current density–length product decreased. The statistical distribution of the critical volume fits the sigma curve well. Lower jL^2 values show large sigma values because of back-stress-induced TTF (time-to-fail) dispersion. A simplified equation is proposed to analyze the experimental data from various combinations of current density and line length at a certain temperature. The resulting threshold–length product $(jL)_C$ value appears to be temperature dependent, decreasing with an increase in temperature in a range of 250–300 °C.

1. Introduction

The enhanced atomic displacement and the accumulated effect of mass transport under the influence of electron wind is known as electromigration (EM) which is a critical wear-out mechanism in copper metallization, limiting the lifetime of interconnect systems. EM failure leads to void formation at the cathode, and extrusion at the anode. It has been found that shorter Al wires are substantially less susceptible to EM damage than longer lines when stressed under the same conditions. This is called the short-length or Blech effect [1]. Blech reported that the electromigration flux transports atoms toward the anode, where the compressive stress, as well as the atom concentration, accumulates. This accumulation increases the chemical potential of Al to such a level that further transport of the atoms to the anode is impossible. In other words, the electrical driving force is balanced by a compressive stress gradient, which causes an equal but opposing driving force. The atomic flux (J) is the result of two opposing driving forces. The net atomic flux is expressed as follows:

$$J = C\frac{D}{kT}\left(Z^* ej\rho - \frac{\Omega\Delta\sigma}{L}\right) \tag{1}$$

where C is the concentration of atoms, D is the diffusivity, k is Boltzmann's constant, T is temperature, Z^* is the effective charge number, e is the fundamental electric charge, ρ is the electric resistivity, j is the current density, Ω is the atomic volume, $\Delta\sigma/L$ is the EM-induced average stress gradient between the anode and the cathode, and L is the metal line length. From Eq. (1), the first term is the electron wind force that moves the ions in the direction of the electron flow, and the second term is the back-stress that pushes the ions in the opposite direction. Once the back-stress gradient balances the EM-driven force, there is no

* Corresponding author. Address: Department of Electronics Engineering, National Chiao-Tung University, Hsin-Chu, Taiwan. Tel.: +886 3 578 9158x33923.
E-mail address: mhlin.ee91g@nctu.edu.tw (M.H. Lin).

0026-2714/$ - see front matter © 2007 Elsevier Ltd. All rights reserved.
doi:10.1016/j.microrel.2007.10.007

net mass transport. The critical current density and line length product is given by

$$(jL)_C = \left(\frac{\Omega\Delta\sigma}{Z^*\rho}\right) \quad (2)$$

Then, Eq. (1) can be further rearranged as

$$J = C\frac{D}{kT}Z^*e\rho[jL - (jL)_C]1/L \quad (3)$$

Blech also found that $(jL)_C$ is a constant for a given temperature and increases at decreasing temperatures in a range of 200–350 °C on Al films.

A question remains whether Cu dual-damascene interconnects exhibit a short-length effect. A reasonable argument was proposed to dispute the validity of this effect [2]. The dual-damascene Cu via is connected to the metal (M2) trench above and separated from the metal (M1) trench below by a thin diffusion barrier to form a flux divergence. A very small mass material depletion at the cathode via may cause an open circuit before a substantial back-stress develops at M2. In this case, the short-length effect would not occur, causing a serious interconnect design complication for dual-damascene Cu process microelectronics [3]. However, the Cu/cap dielectric interface is the dominant diffusion path in Cu damascene interconnects; mass transport in the trench along the interface can surpass via bottom depletion such that steady-state back-stress development will counteract EM-induced via or line failure. The short-length effect will then occur, but the criteria will require conditions that allow sufficient time for significant mass transport prior to steady-state back stress. An experimental complication exists because of potential EM damage in the dual-damascene Cu via/line interface where the weak point may require very little EM-driven material depletion at the cathode via prior to steady-state back stress development [4]. The electromigration short-length effect depends critically on sample configurations and processing. The early failure rate at the via/line interface must be minimized to demonstrate this phenomenon. These concerns have provided the impetus for this investigation into the short-length effect on an electroplated Cu dual-damascene process.

In this work, the short-length effect on a dual-damascene Cu process and its temperature dependence was investigated by using a technologically realistic three-level interconnect structure. The dual-damascene Cu process was optimized for mass production following high quality integration development. An alternate means of determining the threshold–length product $(jL)_C$ value, a model that relates it to the failure volume and atomic flux is proposed. Moreover, this alternate method allows j_C to be estimated. A higher threshold–length value was obtained at 300 °C compared to previous works. A test was performed for a greatly extended time period to examine the extracted $(jL)_C$ values and verify the immortality of Cu/low-k interconnects.

2. Experimental detail

The EM tests were carried out at the package level. Samples were fabricated using a 90 nm Cu dual-damascene process on 300 mm wafers. The film stacks in the test structures were fabricated using a dual-damascene process in which both the via and line were etched into the low-k dielectric followed by backfilling with a liner, a Cu seed, and electroplated Cu. The excess Cu and liner films were removed using a chemical mechanical polishing process. The TaN/Ta liner and Cu seed layers were deposited sequentially by using physical vapor deposition (PVD). In addition, resputtering leads to excellent side wall coverage and void-free vias. The resistance across the test structure was measured in real time using a four-point measurement technique to monitor the electromigration damage in each sample. The EM failure criterion was defined as a 10% increase in resistance, or when the extrusion monitor current exceeded 1 μA. Fig. 1 is a schematic diagram of the three-level interconnects structure discussed in this paper. Line lengths from 5 to 400 μm were used to examine the effect of EM induced back flow. The down-stream case was defined as a condition where the electrons flow from the upper wide metal line over the via and into the narrow metal line below. While, the up-stream case was defined as a condition where the electrons flow from the lower wide metal line under the via and into the narrow metal line above. More than 20 samples were used for each EM test. Stress temperatures were in the range of 250–350 °C (typically 300 °C) in a controlled environment with nitrogen. To determine the effect of Joule heating, sample resistance was measured as a function of current and temperature. The difference between the increase in sample resistance that occurs during the stressing (high) current and the measuring (low) current is attributed to an increase in temperature due to the Joule heating effect. The stressing applied current ranged from 0.4 to 24 mA; the measuring current was 0.1 mA. The sample temperatures ranged from 25 to 350 °C. The relationship between the metal resistance and the temperature is given by $\mathrm{TCR}(T) = [1/R(T)]\ \Delta R/\Delta T$, where TCR is the temperature coefficient of resistance, R is the resistance, and T is the sample temperature. TCR

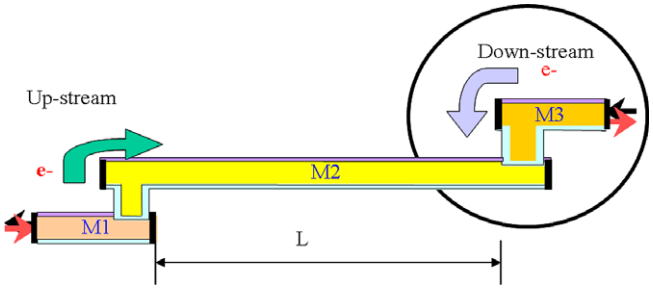

Fig. 1. Schematic diagram of the 0.14 μm wide three-level via terminated line structure. The stripe length L is 5, 10, 25, 50, 100, 200, or 400 μm. Stress direction is defined by electron current flow direction. Down-stream is evaluated in this study.

was determined by measuring the resistance in 50 °C increments in a range from 50 to 300 °C. The correlation between R and T within the investigated temperature range was approximately linear. The average TCR value has been estimated to be 0.0030 ± 0.00016/°C from 271 samples, whose line widths were at 0.14 μm, for a specific process. Reduced stress current densities in the range of $0.6–2.0 \times 10^6$ A/cm^2 (defined with respect to the cross section of the metal line) were used to limit the increase in temperature due to Joule heating to less than 3 °C, even for low-k materials known to possess a small thermal conductivity. Testing was typically conducted at 300 °C at a current density of 1.6×10^6 A/cm^2.

3. Results and discussion

It has been well-established that the back-stress force becomes stronger at lower current densities (j) and shorter line lengths (L) [5]. The maximum stress sustainable between the cathode and anode ends of a line is related to the mechanical strength of the interconnect material and the surrounding dielectric layer, which is related to the material properties, and is not dependent on the length of the metal lines. Therefore, the maximum stress gradient, and thus the back-stress force, is higher for shorter metal lines. As a result, the net EM flux and the rate of resistance increase are smaller for shorter metal lines. The EM critical length effect was evaluated using test structures of various lengths. The cumulative lifetime data for lines of 25–400 μm in length, fitted using a log–normal distribution, are shown in Fig. 2. The EM behavior for different line lengths was evaluated to reveal the influence of back-stress force on line length. The median-time-to-fail (MTF) and TTF distributions of the two line lengths (200 and 400 μm) are very similar indicating the possibility of similar mechanical stress. That is, back-stress force seems to be insufficient to change the failure time under the testing failure criteria used in this study. However, a careful inspection of the plot shows that the TTF distribution of a 50 μm line is wider than that of other lines, and a small percentage of the samples did not fail. The slope of the log–normal plot is almost similar for both 200 and 400 μm length, but is quite different for a 50 μm length structure. A similar short length effect on TTF distribution was observed by Vairagar et al. [6]. The parameter "sigma" is the inverse slope of a log–normal distribution. The log–normal sigma parameter is a measurement of the variation in failure times. As failure times become more widely distributed, sigma must increase. Physically, as the stress current density (j) is very close to the critical current density (jc), the failure time becomes infinite, so that failure does not occur when $j < jc$. In reality, j can be viewed as a statistical parameter because of variations in metal line width and thickness induced by the manufacturing process. There maybe some samples that are stressing at a larger current density, while some samples are stressing low or close to jc. Actually, we found the percentage of non-failure samples (i.e., the resistance increase is very small and below the failure criteria) increases as the jL becomes closer to $(jL)_C$, which indicates that the stress current density variation significantly impacts the lifetime of the interconnect under lower conditions. It is clear that a lower stress current density will cause a large variation of the failure time. Similar current density dependence of sigma was also observed in Al-based technology [7]. The values of sigma in the log–normal distribution versus the jL^2 product are plotted in Fig. 3. An alternate complex mathematic method was used

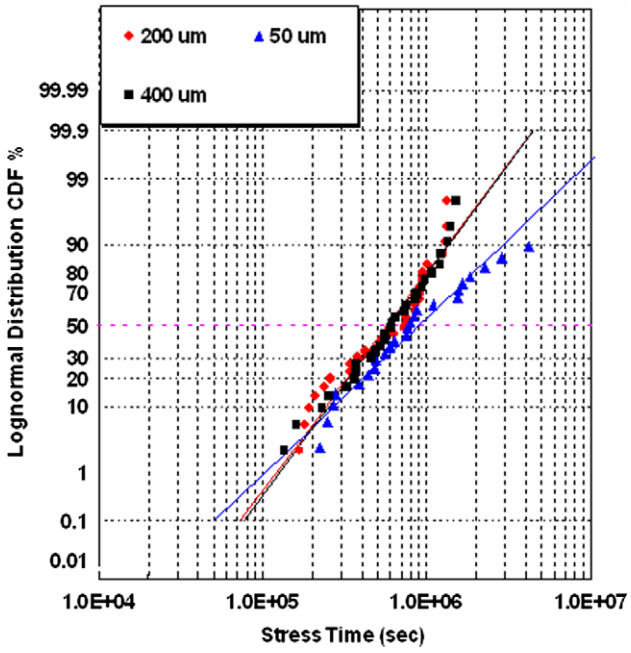

Fig. 2. Log–normal time-to-failure plots for $L = 50$, 200, and 400 μm for down-stream case. Similar TTF distributions are shown for 200 and 400 μm, but wider distribution was found for $L = 50$ μm. EM fail time obtained at 300 °C under current density of 1.6×10^6 A/cm^2.

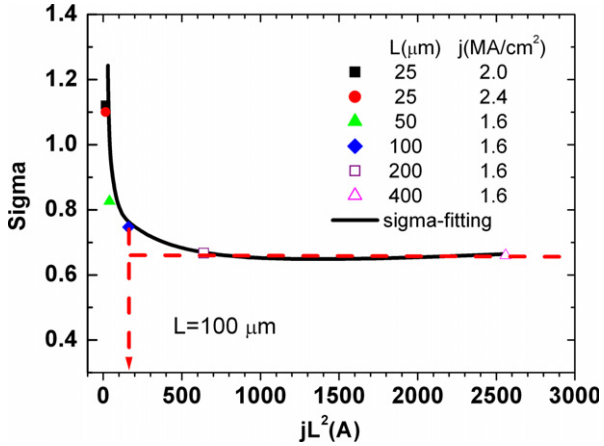

Fig. 3. The sigma of log–normal distribution versus jL^2. Smaller jL^2 values show large TTF dispersion. The solid curve is plotted using the statistical distribution of the critical void volume. A dotted red line to indicate the sigma deviation as the line length is decreased to 100 μm under certain stress conditions. (For interpretation of the references to color in this figure legend, the reader is referred to the web version of this article.)

to fit this dependence. The fitting curve is plotted using a statistical distribution of the critical void volume [8]. He et al. reported that the void volume (V) is a function of time under EM stressing

$$\frac{V}{V_{\text{satu}}} = 1 + \frac{32}{\pi^3}\sum_{n=1}^{\infty}\frac{(-1)^n}{(2n-1)^3}\exp\left[-\left(\frac{2n-1}{2}\pi\right)^2\frac{t}{\tau}\right] \quad (4)$$

where $\tau = (L^2kT)/(DB\Omega)$ and $V_{\text{satu}}=(AZ^*e\rho jL^2)/(2B\Omega)$.

The fail data (t_i) is the time below which i percent of lines in a group fail lie, and the critical voids (V_i) is the volume below which i percent of the critical voids lie. The i percent of the critical voids (V_i) was obtained using Eq. (6). The constants $(kT)/(DB\Omega)$ and $(AZ^*e\rho)/(2B\Omega)$ in V_{satu} and τ were fitted using three sets of EM data (t_{50}, j, L) based on Eq. (6). These sets of t_{50s} were obtained from three structures where the line length (L) was equal to 50, 100, and 200 μm, and were conducted at 300 °C with a current density of 1.6×10^6 A/cm^2. The TTF data from the $L=$ 200 μm structure is used to calculate the V_i. He et al. assume that V_i is independent of testing conditions and test structure lengths. Once the V_i was obtained, the t_i and sigma of $\ln(t_i)$ as a function of j and L can be predicted. The predicted and experimental sigma of $\ln(t_i)$ are plotted in Fig. 3. The sigma for the experiment data shows an abrupt increase as jL^2 approaches zero, and remains constant as jL^2 increases. These results agree with the predicted model. A lower jL^2 product shows larger sigma values as a result of the back-stress-induced TTF dispersion. As the line length is increased to more than 200 μm, the sigma appears to decrease slightly. To avoid the Blech effect, the length of the EM test structure should be greater than 200 μm at a moderate stress current. A relative resistance versus time plot, shown in Fig. 4, further indicates that TTF dispersion is enhanced by back-stress force in line lengths below 50 μm. The relative resistance change becomes saturated at around 103% for $L=25$ μm, while an abrupt resistance change is shown for lengths greater than 100 μm. The

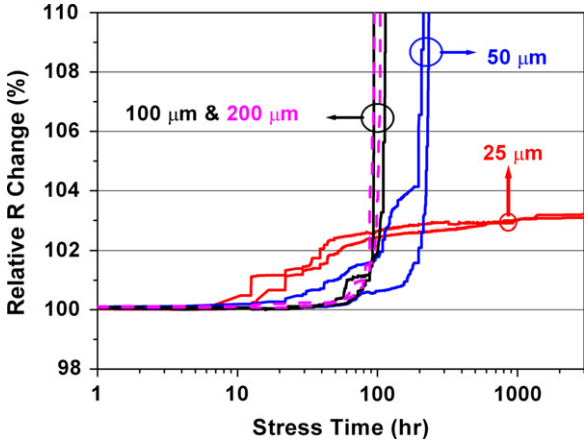

Fig. 4. Relative R change versus time plots for $L=25$, 50, 100 and 200 μm. Two resistance evolution modes were shown, one is the abrupt resistance change, the other is a resistance saturation during the Blech effect. Stress conditions are the same.

change in behavior between the various lengths can only be the result of different rates of void growth. Since the results shown in Fig. 4 correspond to the same electromigration stress conditions, the first term of Eq. (1) can be assumed to be the same for the various lengths. Longer lines increase in resistance at a faster rate than shorter lines. This behavior implies that the net Cu drift velocity must increase as the line length increases, and can only occur if the second term of Eq. (1), the back-stress gradient, is smaller for longer lines in comparison to shorter lines. The results in the present work show that the increase in resistance in long lines, i.e., the amount of EM-induced damage on resistance degradation, is higher than the increase in resistance in short lines. The results are consistent with the work of Korhonen et al. [5], who theoretically showed that the EM-induced stress gradient in finite lines initially decreases from the region of accumulation. Only for longer times does the stress gradient approach a constant value. In addition, for a given time the stress gradient is smaller for long lines compared with short lines. Since it takes a longer time to reach a given back-stress gradient at the cathode end in longer lines, there will be more EM damage. When the opposing back-stress gradient approaches a constant value, the amount of EM damage begins to decrease. It can be noticed in Fig. 4 that the time of resistance onset (e.g., R increase of 1%) decreases as L decreases. A substantial back-stress force quickly develops in a short length line, which then suppresses increase in the resistance. The resistance saturation is a result of a reduction in the rate of EM damage because of the short-length effect. The length-dependent results seen in Fig. 4 are a direct result of the EM short-length effect, and is consistent with current knowledge of the EM short-length effect.

To estimate interconnect lifetime at normal operating conditions, reliability experiments are often based on tests conducted at accelerated conditions (i.e., high temperature and high current densities). If the failure mechanism is the same for both the accelerated and standard design rule operating conditions, the data is scaled back to design rule conditions (i.e., low temperature and low current density). This extrapolation is commonly based on Black's empirical equation [9]

$$\text{MTF} = Bj^{-n_1}\exp\left(\frac{Ea}{kT}\right) \quad (5)$$

where B is the material and geometry constant, and n_1 is the current density exponent. Black's empirical equation introduces the parameter n as a constant value. It has been established through studies on Al interconnects that void-growth-limited failure is represented by a current exponent of 1 [10], while void-nucleation-limited failure is represented by a current exponent of 2 [11]. These concepts appear to be consistent in Cu interconnects where correlations have been made between the n value and the failure analysis [12]. For Cu interconnects, the industry prefers to assume n is close to 1 as a result of void-growth dominating the degradation process. However, this theoretical value is rarely obtained.

Higher n values are obtained using a simple current exponent relation in Black's empirical equation, and depend on jL conditions. From a physical and theoretical point of view, an n value larger than 2 is unusual and is only considered as a fitting parameter. The Blech effect may explain n value that is significantly higher than 1 for lower jL conditions. For longer lines or higher stress current densities, which correspond to higher jL products, an n value close to the common value of 1 is achieved due to the limited back-stress force inside the line. The n value increased significantly for shorter line lengths [13]. Higher n values can be related to significant back-stress in shorter length lines. It will be shown later that the MTF at relatively small current densities does not obey Black's empirical equation. Rather, the MTF data appears to obey a modified Black's empirical equation [14]

$$\mathrm{MTF} = C(j - jc)^{-n_2} \exp\left(\frac{Ea}{kT}\right) \tag{6}$$

where C and n_2 are analogous to B and n_1 in Eq. (5), and j_C is the critical current density. The current exponent n value from Eq. (5) can be correlated to the failure mechanism on the metal interconnects. Fig. 5 shows a log–log plot of the MTF versus the current density–length product for 50 and 400 μm. The stress temperature is 300 °C. Fitting the MTF data for $L = 50$ μm to Eq. (5), and assuming that the exponential term is constant, a linear regression yields a current exponent of $n_1 \approx 1.4$ for a high current density–length product, as indicated by the dashed line. This value is very close to the extracted value of 1.36 for $L = 400$ μm. The observed n value (~1.4) indicates that certain lines in this population suffered failures that were void-growth-limited, while the failures in other lines were void-nucleation-limited. However, as the current density–length product is reduced, the data deviates from the fitting line, and Black's empirical equation is no longer valid (where B and n_1 are the two parameters). The MTF data

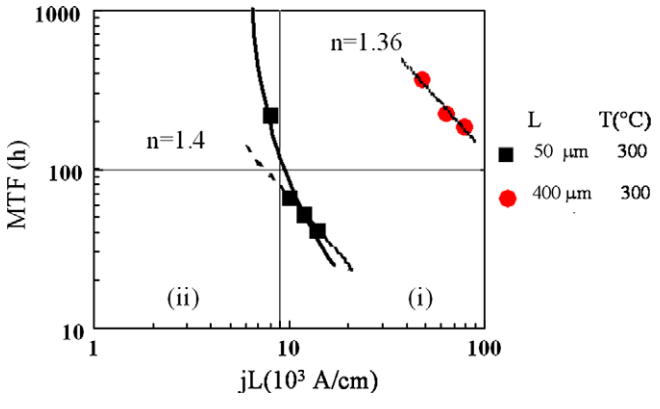

Fig. 5. Log–log plot of MTF versus current density–length product for $L = 50$, 400 μm at 300 °C. The solid line was obtained by fitting the MTF data into Eq. (5), where the regression found $(j_C L) = 6000$ A/cm and $n_2 = 1.2$. The dashed lines indicate $n = 1.4$, 1.36 which fitting the MTF data of $L = 50$, 400 μm to Eq. (4) and assuming that the exponential term is constant, a linear regression yields a current exponent of $n_1 \approx 1.4$, 1.36, respectively, at high current density–length product.

for low current density–length products are better represented by a modified Black's empirical equation Eq. (6), which introduces a third parameter j_C. Eq. (6) states that j_C is a critical current density. If the stress current density is below j_C, the samples will not suffer a failure. The solid line shown in Fig. 5 was obtained by fitting the MTF data for $L = 50$ μm to Eq. (6) with a least-squares nonlinear regression. The regression found that $(j_C L) = 6000$ A/cm and $n_2 = 1.2$. The difference in the relationship between MTF and jL can be separated by a distinct boundary. One region (i) is the EM behavior following Black's equation and has no significant back-stress. The other (ii) is EM behavior that can be better represented by a modified Black's equation, and includes significant back-stress.

As an alternate means of determining the threshold–length product $(jL)_C$ value, a model that relates it to the failure volume and atomic flux is proposed. It is assumed that the electron flow is from the V2 via to the M2 line, the Ta/TaN liner at the V2/M2 interface stud acts as barriers against Cu diffusion, and the atomic flux divergence at the cathode end of the interconnect is expected during EM. Once an electric current is applied to the line, the majority of its lifetime is taken up by expanding the void, while the time required to nucleate the void is neglected. When a period of time equal to the MTF, the depleted atoms occupy a volume equal to the failure volume, V_{fail} [15], which is assumed to be independent of testing variables, such as electric current density, and is constant for the same line length. The MTF can be extrapolated using the following expression:

$$V_{\mathrm{fail}} = JA\Omega * (\mathrm{MTF}) \tag{7}$$

where J is the atomic flux as expressed in Eq. (1), A is the metal line cross-sectional area, and Ω is the atomic volume. Note that at a given temperature and metal line length, V_{fail}, A, and Ω are constants representing the material properties. In the assumptions made in this study, the MTF is inversely proportional to the atomic flux J. Therefore, Eq. (7) can be rearranged as

$$1/(\mathrm{MTF}) = A\Omega V_{\mathrm{fail}} J \propto J$$
$$= C\frac{D}{KT} Z^* e\rho[jL - (jL)_C]1/L \tag{8}$$

Similar relationships between the MTF with respect to the product of jL have been reported by others [16,17]. The threshold–length product $(jL)_C$ value can then be precisely determined. Figs. 6a and b shows the L/MTF versus the current density–length product. A linear relationship between (jL) and L/MTF is indicated by the linear extrapolation to zero. The intercepts with the x axis determined from the linear extrapolation are the $(jL)_C$ values that yield infinite MTF values. Therefore, these intercepts determine the threshold–length products, $(jL)_C$, below which there is no electromigration-induced resistance degradation at their corresponding temperatures. The threshold–length products, $(jL)_C$, determined from Fig. 6a are 10,914 A/cm at 250 °C, 10,278 A/cm at 275 °C, 6675 A/cm at 300 °C for

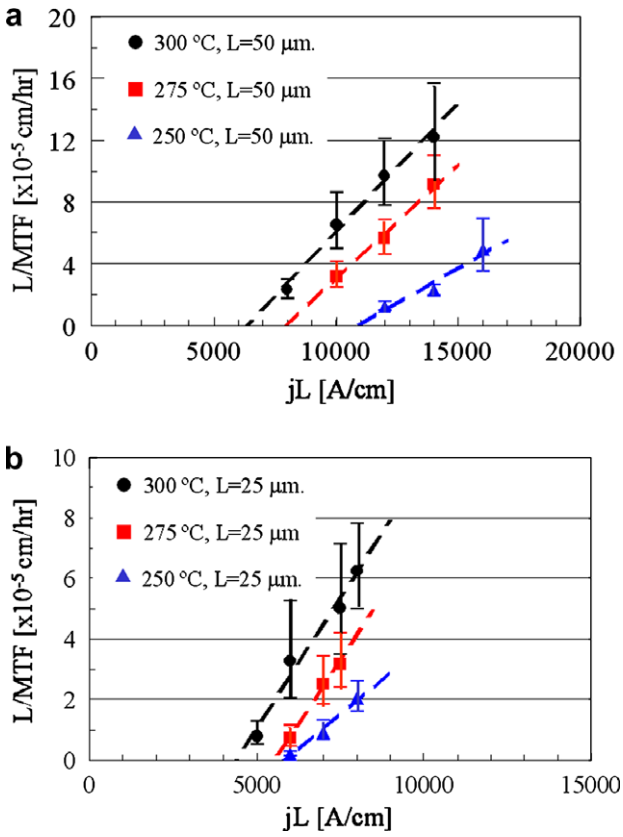

Fig. 6. (a) L/MTF versus current density–length product for $L = 50$ μm. The threshold–length products $(jL)_C$ was calculated to be 6319 A/cm for 300 °C. (b) L/MTF versus current density–length product for $L = 25$ μm. The threshold–length products $(jL)_C$ was calculated to be 4314 A/cm for 300 °C. Error bars represent 90% confidence intervals.

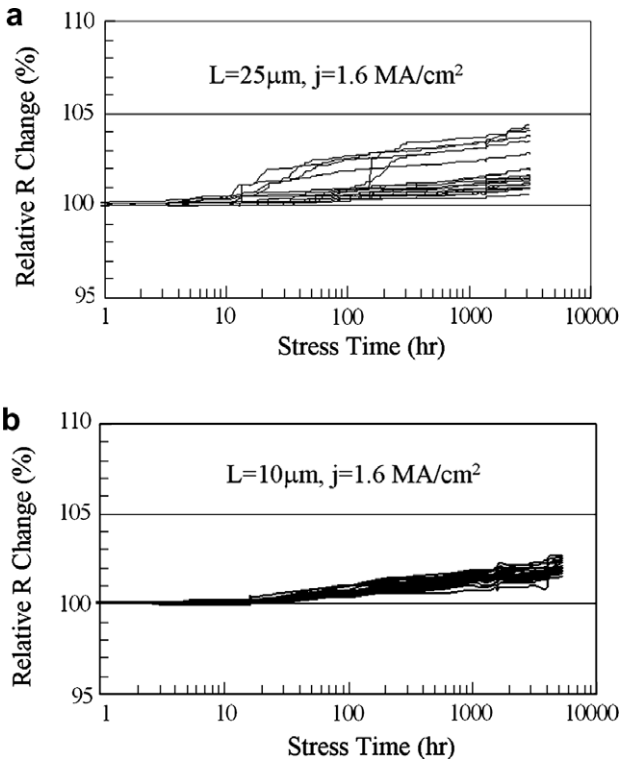

Fig. 7. (a) Relative R change versus time shows slight resistance increase up to 5100 h of testing for $L = 25$ μm, $j = 1.6 \times 10^6$ A/cm^2, $T = 300$ °C, and sample size over 24. The resistance change is very small around 2–4%, show that the immortal behavior occurs, $(jL)_C > 4000$ A/cm. (b) Relative R change versus time shows slight resistance increase up to 5100 h of testing for $L = 10$ μm, $j = 1.6 \times 10^6$ A/cm^2, $T = 300$ °C, and sample size over 24. $(jL)_C > 1600$ A/cm.

$L = 50$ μm, and from Fig. 6b are 5806 A/cm at 250 °C, 5530 A/cm at 275 °C, 4314 A/cm at 300 °C for $L = 25$ μm. The value of $(jL)_C = 6675$ A/cm at 300 °C for $L = 50$ μm is consistent with the regression value $(j_C L) = 6000$ A/cm from Eq. (6). The discrepancy in the threshold–length product for 50 mm and 25 mm lines is noted in this paper and a possible mechanism is proposed based on work conducted by Clement et al. [18]. For a conduct where the material accumulation at the anode end does not produce hillock formation, jc may be proportional to the size of the void formed at the cathode end, which we feel is a reasonable assumption and, although we do not currently have the evidence to show it, that the difference in $(jc)L$ values between 25 and 50 μm can be attributed to a larger critical void size of 50 μm. The dependence of the threshold–length product on the length is also shown in Al metallization, but the $(jL)_C$ value increases as the line length decreases [14]. This may possibly be an ideal topic for investigation in future work. A higher value for the threshold–length product $(jL)_C$ was obtained in this work compared to previous studies. For example [17], achieved 4900 A/cm for low-k dielectrics, using 90 nm technology, a SiCN capping layer, a two-level structure, and a similar extraction method [19], obtained a 2000 A/cm for CVD low-k, using 0.5 μm wider metal width, a SiN capping layer, a two-level structure, and a serially connected line/via structure, but employed a statistical extraction method. However [20], achieved 4000 A/cm for oxide, using a 0.245 μm metal width and a similar three-level structure, but considered an incubation period extraction method. In addition, to justify these $(jL)_C$ values, several experiments were conducted under stressing conditions lower than the $(jL)_C$ values at their respective temperatures, e.g., 25 μm lines stressed at 1.6×10^6 A/cm^2 and 300 °C. As expected, and shown in Fig. 7, for those stress samples below the threshold conditions, there is no major resistance degradation during an extended time period up to 5100 h, which shows that immortal behavior occurs when $L = 10$ or 25 μm under these testing conditions. The resistance change is very small around 2–4%. For $L = 25$ μm, the jL product at 300 °C is 4000 A/cm, which further supports the proposed threshold–length extraction method and justifies the $(jL)_C$ values. Extensive failure analysis was carried out to reveal any potential failure mechanisms in the test structures. Fig. 8a shows the FIB images of a metal line 10 μm in length after the passage of 1.6×10^6 A/cm^2 for about 5100 h at 300 °C. No clear void was found at either the anode or cathode ends along the line. A high-resolution TEM was analyzed at the cathode end to reveal the detailed microstructure, as shown in Fig. 8b, which shows

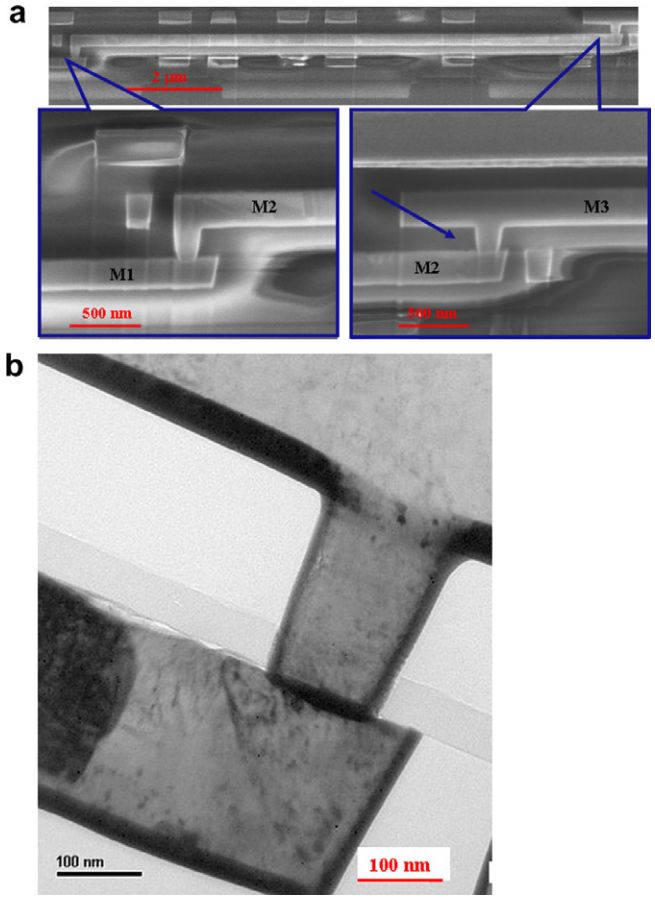

Fig. 8. (a) SEM images for $L = 10\ \mu m$ line structure after passage of $1.6 \times 10^6\ A/cm^2$ for about 5100 h at 300 °C. No clear void was found at the anode or cathode ends along the line. (b) A high-resolution TEM was analyzed at the cathode end to reveal the detail microstructure. Very small void has formed at cathode end, which lead to an only minor resistance increase.

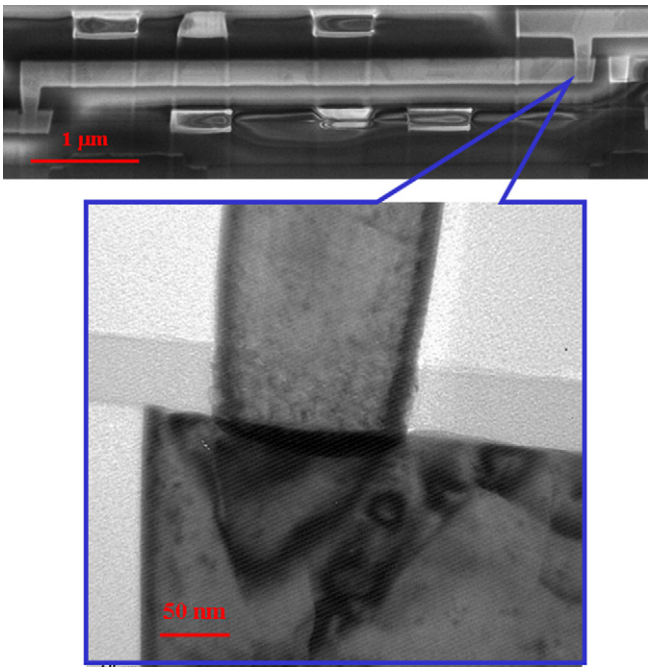

Fig. 9. FIB and TEM images of a stripe 5 μm length after passage of $1.6 \times 10^6\ A/cm^2$ for about 5000 h at 300 °C. The EM-induced void of a stripe 5 μm length is much smaller than that of 10 μm length.

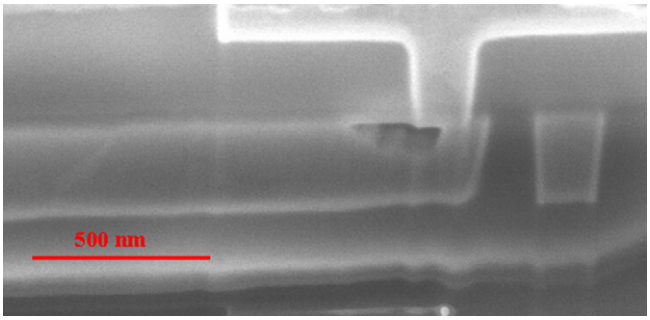

Fig. 10. An example of FIB cross sections at the cathode end along the 25 μm length line after passage of $1.6 \times 10^6\ A/cm^2$ for about 5000 h at 300 °C. The void has partially exposed the bottom of the via.

that a very small void has formed underneath the cap-layer at the cathode end, leading to only a minor increase in resistance. Fig. 9 shows the FIB and TEM images of a metal line 5 μm in length after the passage of $1.6 \times 10^6\ A/cm^2$ for about 5100 h at 300 °C. The EM-induced void of the 5 μm line is much smaller than that of the 10 μm line. These results further support the hypothesis that mass transport in the trench along the interface is able to surpass via bottom depletion such that steady-state back-stress development will counteract EM-induced via or line failure. If (jL) exceeds the critical threshold–length product, void nucleation will occur, but is not necessarily fatal if the void does not completely separate the line from the via. Fig. 10 is an example of a FIB cross-section at the cathode end of a 25 μm metal line. The void has partially exposed the bottom of the via, which likely represents a void-growth-limited failure, since a larger void size is required before the resistance increases to 10%.

The temperature dependence of the threshold–length product is an important consideration for determining critical current densities at standard operating conditions. The temperature dependence of the threshold–length product for 50 and 25 μm lines is shown in Fig. 11, and was found to be a function of the temperature. It is interesting that the jL value increases slowly at low temperatures for both lengths, which can be partly attributed to the temperature-dependent mechanical properties of the system [3,20]. Note that the EM threshold–length product is critically dependent on sample configurations and processing, which in this study, was determined based only on the critical failure volume model. The activation energy was found to be 1.0 for the 50 μm line, which indicates no early failure mechanism affecting the result. It was also noticed that the $(jL)_C$ value needs to be obtained for the standard operating temperature that would be used in possible design implementations, typically around 100 °C. A better understanding of the temperature dependence of the $(jL)_C$ is required. The

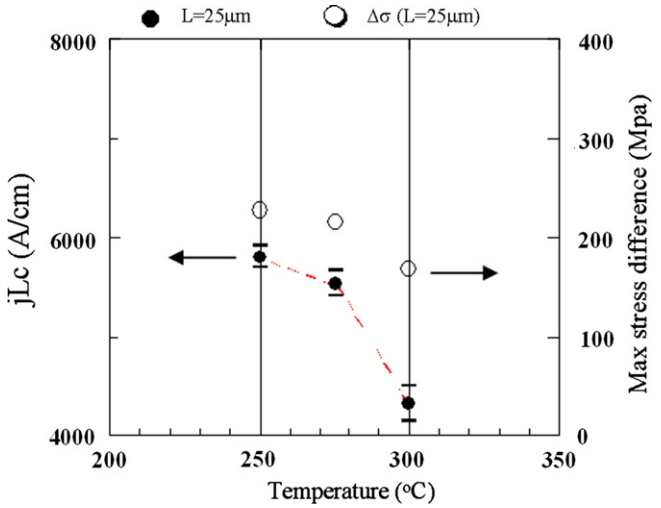

Fig. 11. Temperature dependence of critical length effect and maximum stress difference in the interconnect for $L = 25$ μm. It is observed that jL value increase slowly at low temperature.

maximum stress difference in the interconnects for void nucleation was determined to be 400 MPa at 250 °C. This value represents the tensile stress needed to nucleate a void in the metal. This value is larger than previously reported values, and may indicate differences in the quality of the Cu/cap interface. However, the value is much lower than the critical stress of 600 MPa observed for Al-based interconnect systems [21], which indicates that voids form much more readily in Cu- than in Al-based interconnects.

Finally, We believe that the analysis methods used in the paper can be implemented into Al technology. However, the processing technologies for Al- and Cu-based interconnects are significantly different. In a Ti and/or TiN under- and over-layer sandwich, the Al and serves as an electrical shunt. For Al technology, the resistance shift is small, below 20% in the saturation regime [21]. While for Cu interconnects, the saturation resistance shift is around 10 times larger than Al due to the dielectric capping layer on the top surface. If the capping layer material is metal (e.g., CoWP, Ta, W, ...), it serves well as an electric shunt if the void grows during EM. The Cu-based system is very close to the Al-based system, except for a lower critical stress value as a result of the soft surrounding dielectric material in the Cu-based system. The benefit of the Blech effect is that it allows for higher current densities to be used at standard operating conditions for short interconnects. Practically, the length of an immortal interconnect designed to carry a certain current density can be calculated using the threshold–length product $(jL)_C$. For example, a 10 μm interconnect can sustain around 4×10^6 A/cm^2 at 300 °C without serious degradation as $(jL) = 4000$ A/cm; while a 50 μm interconnect can only sustain about 0.8×10^6 A/cm^2. Another practical design rule methodology was proposed by Filippi and co-workers [22]. An EM resistant power grid may be designed that takes advantage of the short length effect. It should be noted that the threshold–length product depends critically on the sample configuration, such as the surrounding dielectric material, process specifications, etc. Therefore, care must be taken in applying this value for certain interconnect systems.

4. Conclusions

In conclusion, we have investigated the effect of line length scaling on electromigration in dual-damascene Cu interconnects by testing several three-level structures. Different line lengths were evaluated to reveal the back-stress force influence on line length. The values of sigma in the log–normal distribution versus the jL^2 product can be modeled using a statistical distribution of the critical void volume. A lower jL^2 product shows large sigma values as a result of back-stress-induced TTF dispersion. To avoid the Blech effect, the EM test structure length should be longer than 200 μm at moderate stress currents. A relative resistance versus time plot further indicates that TTF dispersion is enhanced by back-stress force at line lengths below 50 μm. Two resistance evolution modes were observed. The percentage of abrupt open-circuit failures was found to decrease as the line length decreases. As the line length decreases to 25 μm, most samples show that the resistance gradually increases over the time evolution. A direct result of the electromigration short-length effect was demonstrated.

The MTF at relatively low current densities does not obey Black's equation. Instead, the MTF follows a modified Black's equation in which MTF $\propto (j - jc)^{-n_2}$ at a constant temperature. The difference in the relationship between MTF and jL can be separated by a distinct boundary. One region (i) is the electromigration behavior following Black equation and has no significant back-stress. The other (ii) is the electromigration behavior that can be better represented by a modified Black's equation, and includes significant back-stress. As an alternate means of determining the threshold–length product $(jL)_C$ value, a model that relates it to the failure volume and atomic flux is proposed. The extracted values are consistent with the regression value from the modified Black's equation, and these $(jL)_C$ value were verified during an extended stress test period. Extensive failure analysis shows that no clear void was found at the anode or cathode ends along the line if (jL) is below the critical threshold–length product, and was found to be a function of temperature. Since the $(jL)_C$ value needs to be obtained for the standard operating temperatures for possible design implementation, there is room for further investigation into the temperature dependence of the $(jL)_C$.

Acknowledgements

The authors would like to acknowledge financial support from National Science Council (NSC), Taiwan under Contract No. NSC94-2215-E009-009. UMC technology development, reliability and failure analysis groups are also

gratefully acknowledged for many helpful comments and great support.

References

[1] Blech IA. Electromigration in thin aluminum films on titanium nitride. J Appl Phys 1967;47:1203–8.
[2] Ogawa ET, Bierwag AJ, Lee KD, Matsuhashi H, Justison PR, Ramamurthi AN, et al. Direct observation of a critical length effect in dual-damascene Cu/oxide interconnects. Appl Phys Lett 2001;78:2652–4.
[3] Thompson CV, Gan CL, Alam SM, Troxel DE, Experiments and models for circuit-level assessment of the reliability of Cu. In: International interconnect technology conference, IEEE; 2004. p. 69–71.
[4] Hau-Riege SP. Probabilistic immortality of Cu damascene interconnects. J Appl Phys 2002;91:2014–22.
[5] Korhonen MA, Borgesen P, Tu KN, Li CY. Stress evolution due to electromigration in confined metal lines. J Appl Phys 1993;73:3790–9.
[6] Vairagar AV, Mhaisalkar SG, Krishnamoorthy A. Electromigration behavior of dual-damascene Cu interconnects – structure, width, and length dependences. Microelectron Reliab 2004;44:747–54.
[7] Oates AS. Electromigration failure distribution of contacts and vias as a function of stress conditions in submicron IC metallizations. In: Proceedings of the 34th annual reliability physics symposium, IEEE; 1996. p. 164–71.
[8] He J, Suo Z, Marieb TN, Maiz JA. Electromigration lifetime and critical void volume. Appl Phys Lett 2004;85:4639–41.
[9] Black JR. Mass transport of aluminum by momentum exchange with conducting electrons. In: Proceedings of the sixth annual reliability physics symposium, IEEE; 1967. p. 148–53.
[10] Kircheim R, Kaeber UJ. Atomistic and computer modeling of metallization failure of integrated circuits by electromigration. J Appl Phys 1991;70:172–81.
[11] Lloyd JR. Electromigration failure. J Appl Phys 1991;69:7601–4.
[12] Hau-Riege CS. An introduction to Cu the electromigration. Microelectron Reliab 2004;44:195–205.
[13] Hau-Riege CS, Marathe AP, Pham V. The effect of low-k ILD on the electromigration reliability of Cu interconnects with different line lengths. In: Proceedings of the 41th annual reliability physics symposium, IEEE; 2003. p. 173–7.
[14] Filippi RG, Biery GA, Wachnik RA. The electromigration short-length effect in Ti–AlCu–Ti metallization with tungsten studs. J Appl Phys 1993;78:3756–68.
[15] Oates AS. Electromigration failure distribution of contacts and vias as a function of stress conditions in submicron IC metallizations. In: Proceedings of the 34th annual reliability physics symposium, IEEE; 1996. p. 164–71.
[16] Thrasher S, Capasso C, Zhao L, Hernandez R, Mulski P, Rose S. Blech effect in single-inlaid Cu interconnects. In: International interconnect technology conference, IEEE; 1991. p. 177–9.
[17] Ney D, Federspiel X, Girault V, Thomas O, Gerqaud P. Electromigration threshold in copper interconnects and consequences on lifetime extrapolations. In: International interconnect technology conference, IEEE; 2005. p. 105–7.
[18] Clement JJ, Lloyd JR, Thompson CV. Failure in tungsten-filled via structures. Mater Res Symp Proc 1995;391:423–8.
[19] Ho PS, Lee K-D, Yoon S, Lu X, Ogawa ET. Effect of low k dielectrics on electromigration reliability for Cu interconnects. Mater Sci Semicond Process 2004;7:157–63.
[20] Wang P-C, Filippi RG. Electromigration threshold in copper interconnects. Appl Phys Lett 2001;78:3598–600.
[21] Hau-Riege CS, Thompson CV. The effects of microstructural transitions at width transitions on interconnect reliability. J Appl Phys 2000;87:8467–72.
[22] Wachnik RA, Filippi RG, Shaw TM, Lin PCV. Practical benefits of electromigration short-length effect, including a new design rule methodology and an electromigration resistant power grid with enhanced wireability. In: Symposium on VLSI technology, Digest of technical papers; 2000. p. 220–21.